JM PAPERS

Non-homogeneous approximation for the kurtosis evolution of shoaling rogue waves

S. Mendes[1,2,†] **and J. Kasparian**[1,2]

[1]Group of Applied Physics, University of Geneva, Rue de l'École de Médecine 20, 1205 Geneva, Switzerland

[2]Institute for Environmental Sciences, University of Geneva, Boulevard Carl-Vogt 66, 1205 Geneva, Switzerland

Bathymetric changes have been experimentally shown to affect the occurrence of rogue waves. We recently derived a non-homogeneous correction to the spectral analysis, allowing us to describe the evolution of the rogue wave probability over a shoal. Here, we extend this work to the evolution of the excess kurtosis of the surface elevation, that plays a central role in estimating rare event probabilities. Furthermore, we provide an upper bound to the excess kurtosis. In intermediate and deep water regimes, a shoal does not affect wave steepness nor bandwidth significantly, so that the vertical asymmetry between crests and troughs, the excess kurtosis and the exceedance probability of wave height stay rather constant. In contrast, in shallower water, a sharp increase in wave steepness increases the vertical asymmetry, resulting in a growth of both the tail of the exceedance probability and the excess kurtosis.

Key words: coastal engineering, surface gravity waves

1. Introduction

Ocean wave statistics is at the crossroads of ocean engineering and physical oceanography. Ocean engineers are commonly concerned with both short-term and long-term wave statistics (Clauss 2002), while the mechanisms responsible for the formation of extreme waves is the focus in physical oceanography (Toffoli *et al.* 2015). The unexpected observation of the so-called rogue waves (also known as freak waves) over the past decades (Haver 2004) reignited the cross-disciplinary interest in wave statistics. These waves seemingly 'appear from nowhere' (Akhmediev, Ankiewicz & Taki 2009), and are

† Email address for correspondence: saulo.dasilvamendes@unige.ch

by statistical definition at least twice taller than the significant wave height. From an engineering perspective, the performance of theoretical probability models at the tail of the wave height distribution measures their practical success and applicability to structure dimensioning.

Applying the signal processing methods of Rice (1945), the bulk of surface gravity waves were demonstrated to follow a Rayleigh distribution of heights (Longuet-Higgins 1952). Nevertheless, the Rayleigh distribution is unsuited to capturing the tail of the distribution in real ocean conditions (Forristall 1978; Tayfun 1980). On the other hand, nonlinear theories and their associated probability distributions are inaccurate in a wide range of real ocean conditions (Karmpadakis, Swan & Christou 2020; Teutsch *et al.* 2020). These difficulties were realized early on, such that an approach based on the expansion of sums of Gram–Charlier series for a weakly non-Gaussian distribution of the ocean surface (Longuet-Higgins 1963) has been widely favoured. As reviewed in Tayfun & Alkhalidi (2020), the computation of surface elevation, crest and wave height distributions requires methodologies that are often computationally burdensome. Naturally, the excess kurtosis became the centre of wave statistics in an attempt to transfer the problem from the probability distribution to the cumulant expansion (Bitner 1980; Tayfun 1990). The complexity of water wave solutions led to the use of excess kurtosis as a practical alternative to the evaluation of statistical distributions (Marthinsen 1992; Mori & Janssen 2006).

Over the past decade, experiments and numerical simulations have been performed to assess the effect of shoaling of irregular waves on the amplification of rogue wave intensity and occurrence (Trulsen, Zeng & Gramstad 2012; Raustøl 2014; Ma, Ma & Dong 2015; Ducrozet & Gouin 2017; Bolles, Speer & Moore 2019; Zhang *et al.* 2019; Li *et al.* 2021*b*). Trulsen *et al.* (2020) provided experimental data with the broadest set of conditions and widest range of relative water depths. As reviewed in Mendes & Kasparian (2022), three complementary theoretical models for the wave statistics have emerged, albeit they tend to focus on either the surface elevation (Moore *et al.* 2020), the crest height (Li *et al.* 2021*a*) or the crest-to-trough height statistics (Mendes *et al.* 2022). Although the observed probability of exceedance of rogue waves in the experiments of Trulsen *et al.* (2020) has been well described by the third model (Mendes *et al.* 2022), their observed excess kurtosis has not been addressed yet. To fill this gap, we provide an effective extension to the theory of energy density redistribution (Mendes *et al.* 2022) to describe the evolution of the kurtosis of wave trains travelling over a shoal. Because the increase of the vertical asymmetry between crests and troughs is a key ingredient of the amplification of rogue wave probability over a shoal (Tayfun & Alkhalidi 2020; Mendes *et al.* 2022), we derive an approximation for this asymmetry as a function of water depth, bandwidth and steepness. Variations in vertical asymmetry in intermediate and deep water regimes are too small to affect the amplification of rogue waves travelling past a shoal, unless either the spectrum is significantly broad-banded or the steepness is large. Accordingly, the resulting upper bound for the vertical asymmetry leads to an upper bound for the excess kurtosis, a key piece of information for dimensioning structures as well as for wave forecast (Janssen & Bidlot 2009).

2. Theoretical considerations

We first recall the main ideas of the theory of the non-homogeneous analysis of water waves travelling over a shoal (Mendes *et al.* 2022). Given a velocity potential $\Phi(x, z, t)$ and surface elevation $\zeta(x, t)$ of waves travelling over a horizontally variable water depth $h(x)$, the average energy density evolving over a shoal described by $h(x) = h_0 + x\nabla h$ with
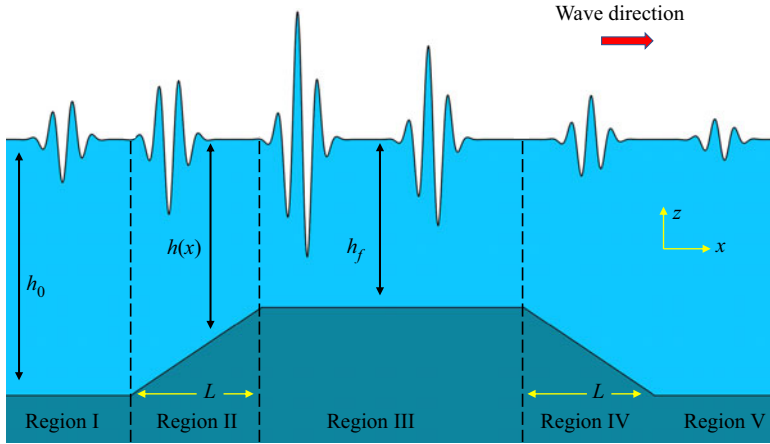
Figure 1. Portrayal of the extreme wave amplification due to a bar (Mendes *et al.* 2022). The water column depth evolves as $h(x) = h_0 + x\nabla h$ with slope $\nabla h = (h_f - h_0)/L$. Dashed vertical lines delineate shoaling and de-shoaling regions as in figure 2.

finite constant slope $1/20 \leq |\nabla h| < 1$ (see figure 1) is expressed as

$$\mathscr{E} = \frac{1}{2\lambda} \int_0^\lambda \left\{ [\zeta(x,t) + h(x)]^2 - h^2(x) + \frac{1}{g} \int_{-h(x)}^\zeta \left[\left(\frac{\partial \Phi}{\partial x} \right)^2 + \left(\frac{\partial \Phi}{\partial z} \right)^2 \right] \mathrm{d}z \right\} \mathrm{d}x, \quad (2.1)$$

with zero-crossing wavelength λ, gravitational acceleration g and we abuse the notation for the projection of the gradient of the depth onto the wave direction $\nabla h \equiv \nabla h \cdot \hat{x} \equiv \partial h/\partial x$. The inhomogeneity of both $\mathscr{E}(x)$ and $\langle \zeta^2 \rangle_t(x)$ redistributes energy among wave heights and transforms their exceedance probability. In the case of an initial Rayleigh distribution in region I of figure 1, over and past the shoal (regions II–V) the exceedance probability reads

$$\mathbb{P}_{\alpha,\Gamma}(H > \alpha H_s) = \int_\alpha^{+\infty} \frac{4\alpha_0}{\Gamma} \exp(-2\alpha_0^2/\Gamma) \, \mathrm{d}\alpha_0 = \exp(-2\alpha^2/\Gamma), \quad (2.2)$$

where the correction arises from the evolution of an inhomogeneous wave spectrum over the shoal (Mendes *et al.* 2022) ($\langle \cdot \rangle_t$ stands for temporal average)

$$\Gamma(x) \approx \frac{\langle \zeta^2(x,t) \rangle_t(x)}{\mathscr{E}(x)}. \quad (2.3)$$

The spectral correction Γ depends on the steepness $\varepsilon = H_s/\lambda$ and depth $k_p h$, with H_s being the significant wave height, defined as the average among the 1/3 largest waves. Note that H_s typically differs by a few per cent from its spectral counterpart $H_{m0} = 4\sqrt{m_0}$ of Gaussian seas (Casas-Prat & Holthuijsen 2010; Mendes, Scotti & Stansell 2021), where m_0 is the variance of the surface elevation $\zeta(x,t)$ computed from the wave spectrum. However, this difference can be as large as 10 % in strongly non-Gaussian seas (Goda 1983; Mendes *et al.* 2022). For linear waves ($\varepsilon \ll 1/100$), $\Gamma = 1$ and we recover the case of a Gaussian sea. When solving Γ for second-order irregular waves, we assume that the shoal is linear ($\nabla^2 h = 0$), the length of the shoal is relatively short ($L/\lambda \lesssim 1$) and we deal with small amplitude waves only ($\zeta/h \ll 1$). These assumptions greatly simplify the problem, but are also representative of real ocean bathymetry

(Mendes & Kasparian 2022). Furthermore, we have recently demonstrated that as the slope magnitude increases the rogue wave occurrence follows suit. However, if we assume a small effect of reflection due to a small surf similarity parameter among spectral components (Battjes 1974), the increase in rogue wave occurrence saturates for slopes larger than or equal to $25°$ (Mendes & Kasparian 2022). The evolution of the exceedance probability $\mathbb{P}(H > \alpha H_s)$ in (2.2) can be generalized to any arbitrary incoming statistics (Mendes *et al.* 2022)

$$\mathbb{P}_{\alpha, \Gamma_{\mathfrak{S}}} \approx (\mathbb{P}_{\alpha})^{1/\mathfrak{S}^2 \Gamma_{\mathfrak{S}}} \quad \therefore \quad \ln\left(\frac{\mathbb{P}_{\alpha, \Gamma_{\mathfrak{S}}}}{\mathbb{P}_{\alpha}}\right) \approx 2\alpha^2 \left(1 - \frac{1}{\mathfrak{S}^2(\alpha)\Gamma_{\mathfrak{S}}}\right), \qquad (2.4)$$

with the vertical asymmetry between crests and troughs being defined as twice the ratio between crest and crest-to-trough heights (Mendes *et al.* 2021),

$$\mathfrak{S} = \frac{2\mathcal{Z}_c}{H} \quad \therefore \quad 1 \leq \mathfrak{S} \leq 2, \qquad (2.5)$$

which for rogue waves features the mean empirical value

$$\mathfrak{S}(\alpha = 2) \approx \frac{2\eta_s}{1 + \eta_s}\left(1 + \frac{\eta_s}{6}\right), \qquad (2.6)$$

where η_s measures the ratio between mean crests and mean troughs and has empirically been found in a wide range of sea conditions to depend on the skewness of the surface elevation μ_3 (Mendes *et al.* 2021)

$$\eta_s \approx 1 + \mu_3. \qquad (2.7)$$

The empirical relations of (2.6), (2.7) stem from field observations during North Sea storms detailed in § 4. When the water depth decreases waves become steeper while the super-harmonic contribution has an increasing share of the wave envelope. The combination of these two effects redistributes the exceedance probability by causing the rise in $\langle \zeta^2 \rangle$ to exceed the growth of $\mathscr{E}$. Such uneven growth explains why a shoal in intermediate water amplifies rogue wave occurrence as compared with deep water (Trulsen *et al.* 2020; Kimmoun *et al.* 2021) while it reduces this occurrence in shallow water (Glukhovskiy 1966; Karmpadakis, Swan & Christou 2022). The linear term in $\zeta(x, t)$ has the leading order in deep water and $\Gamma - 1 \lesssim 10^{-2}$ is small. Conversely, in intermediate water the super-harmonic creates significant disturbances in the energy density increasing $\Gamma - 1$ up to 10^{-1}, whereas in shallow water the super-harmonic diverges and $\Gamma - 1 \lesssim 10^{-3}$ becomes small again, reading even smaller values than in deep water.

3. Kurtosis evolution over a shoal

The probability evolution of (2.2) depends solely on Γ. Any deviation from a Gaussian distribution may be described by a cumulant expansion (Longuet-Higgins 1963) which at leading order is expressed as a function of the excess kurtosis μ_4. For the case of an inhomogeneous wave field due to a shoal, there is an excess in kurtosis due to the energy partition. To avoid the tedious algebra of equations (C1,C7b,C12) of Mendes *et al.* (2022) for the case of a non-Gaussian sea prior to the shoal, we consider the probability ratio relative to the Rayleigh distribution (implying a pre-shoal $\mu_4 = 0$) to obtain the excess kurtosis. The ratio measures the amplification of the exceedance probability of waves with height $H = \alpha H_s$ due to a shoal and is computed through the transformation of variables

from the wave envelope in Mori & Yasuda ([2002](#)) into normalized heights to leading order in μ_4, as computed in § 6.2.3 of Mendes ([2020](#))

$$\frac{\mathbb{P}_{\alpha,\mu_4}}{\mathbb{P}_\alpha} \approx 1 + \mu_4 \cdot \frac{\alpha^2}{2}\left(\alpha^2 - 1\right) + \mu_3^2 \cdot \frac{5\alpha^2}{18}\left(2\alpha^4 - 6\alpha^2 - 3\right), \quad \forall\, \alpha \geq 1. \quad (3.1)$$

Taking into account the theoretical relation $\mu_4 \approx 16\mu_3^2/9$ between kurtosis and skewness for waves of second order in steepness confirmed by wave shoaling experiments (Mori & Kobayashi [1998](#)), we rewrite (3.1)

$$\frac{\mathbb{P}_{\alpha,\mu_4}}{\mathbb{P}_\alpha} \approx 1 + \mu_4 \cdot \frac{\alpha^2}{32}\left(10\alpha^4 - 14\alpha^2 - 31\right), \quad \forall\, \alpha \gtrsim 2. \quad (3.2)$$

The kurtosis measures tailedness and it affects the exceedance probability for $\alpha \gtrsim 1.5$. Equations (2.4) and (3.2) both describe the same consequence of energy redistribution and the associated deviation from a Gaussian sea, but the former embodies the physics of shoaling while the latter delineates the perturbation on the statistics regardless of the physical mechanism. Therefore, they can be matched, yielding a kurtosis $\mu_4(\Gamma, \alpha)$. This matching could be performed at any value $\alpha \geq 1.5$, however, higher accuracy is obtained in the region of stability of the approximation ($2 \lesssim \alpha \lesssim 3$). Over this range, the resulting value of μ_4 deviates by less than 20 %. Therefore, we match both equations at $\alpha = 2$ without substantial loss in precision

$$\mu_4(\Gamma) \approx \frac{1}{9}\left[\exp\left(8\left(1 - \frac{1}{\mathfrak{S}^2\Gamma}\right)\right) - 1\right]. \quad (3.3)$$

This expression generalizes the result obtained by (46)–(47) of Mori & Janssen ([2006](#)) in the case of a narrow-banded wave train, with less than 5 % deviation as compared with their model with a $(2/3)\alpha^2(\alpha^2 - 1)$ polynomial in the counterpart of (3.2) for small values of the skewness ($\mu_3 \ll 1$). However, if the surface elevation is significantly skewed ($\mu_3 \gtrsim 1$) the contribution of the skewness is severely underpredicted by (46)–(47) of Mori & Janssen ([2006](#)) and therefore the excess kurtosis will be overpredicted while describing the ratio $\mathbb{P}_{\alpha,\mu}/\mathbb{P}_\alpha$.

In order to validate our effective theory for steep slopes of (3.3), figure 2 compares its prediction with the observed excess kurtosis in Trulsen *et al.* ([2020](#)). In the comparison, we employed the empirical (Mendes *et al.* [2021](#)) asymmetry $\mathfrak{S}(\alpha = 2) = 1.2$. We shall validate this approximation in the next section in relative water depth $k_p h \gtrsim \pi/10$, bandwidth $\nu \lesssim 1/2$ as defined in Longuet-Higgins ([1975](#)) and steepness $\varepsilon \ll 1/10$ representative of Trulsen *et al.*'s experiments. In these experiments, irregular waves with a broad-banded Joint North Sea Wave Project spectrum of $\gamma = 3.3$ peak enhancement factor, significant wave height 1.4 cm $< H_s <$ 3.4 cm and peak period 0.7 s $< T_p <$ 1.1 s were generated in a 24.6 m long and 0.5 m wide unidirectional wave tank. These irregular waves travelled over a flat bottom that had initial relative water depth ranging from $k_p h = 4.9$ (deep water) to $k_p h = 1.8$ (intermediate water). Furthermore, the irregular waves propagated over a symmetrical breakwater as sketched in figure 1 with slope $|\nabla h| \approx 1/3.8$ on each side and located 10.8 m after the wavemaker, or equivalently half a dozen peak wavelengths. The relative water depths atop the shoal are in the range $0.54 \leq k_p h \leq 1.60$. In addition, the absolute water depths ranged from 0.5 to 0.6 m prior to the shoal and from 0.08 to 0.18 m atop the shoal. Equation (3.3) reproduces well the magnitude and the trend of the peak in excess kurtosis to decrease towards deeper waters of the experiments in Trulsen *et al.* ([2020](#)) (see figure 2). Remaining differences such as the slightly earlier rise of
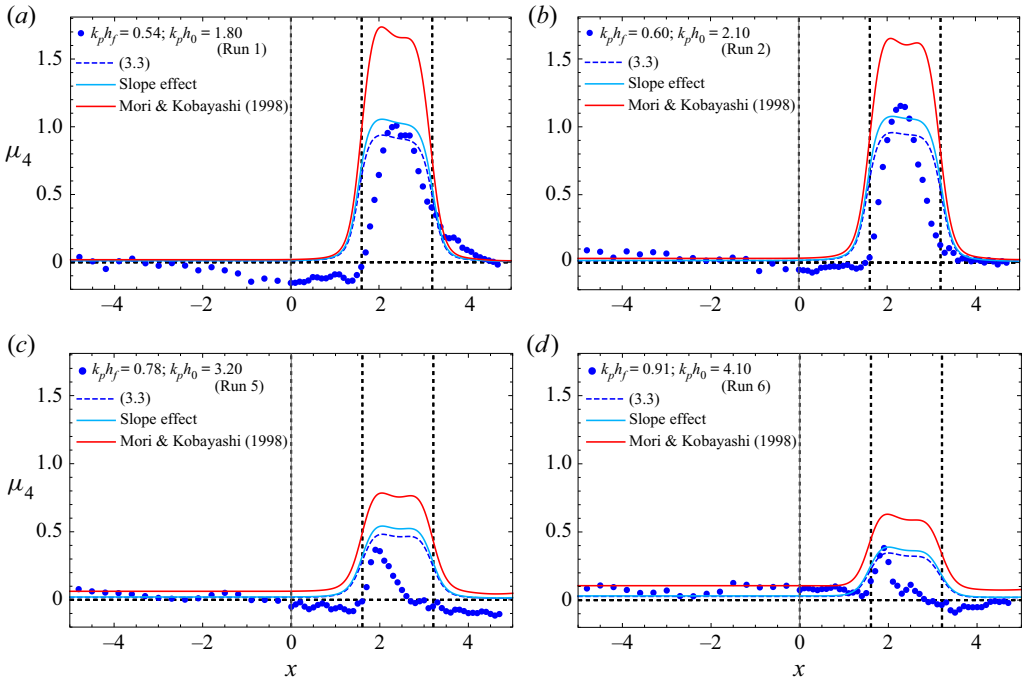
Figure 2. Observed kurtosis μ_4 (dots) vs the model of (3.3) (dashed) for runs 1, 2, 5 and 6 in Trulsen *et al.* (2020). Dashed vertical lines mark the shoaling and de-shoaling zones (see figure 1). The cyan solid curve includes the slope effect (Mendes & Kasparian 2022) while the red solid curve shows the bound wave prediction for the kurtosis according to Mori & Kobayashi (1998).

kurtosis in the shoaling zone and the later fall in the de-shoaling zone are likely due to the assumption of negligible reflection. We also computed the kurtosis contribution due to the bound wave following Mori & Kobayashi (1998) to evaluate its performance over abrupt changes in relative water depth, see Appendix A. This bound kurtosis model (red curve in figure 2) captures the qualitative trend for the observed kurtosis evolution. However, since the latter was developed for a flat bottom and has no explicit slope dependence it overestimates the magnitude of the effect. Furthermore, our model in (3.3) has the advantage of being extendable to any arbitrary slope (Mendes & Kasparian 2022).

4. Wave vertical asymmetry in finite depth

Equations (2.4) and (3.3) highlight the influence of the vertical asymmetry on the evolution of rogue wave occurrence and excess kurtosis of the surface elevation over a shoal in intermediate depths. However, the evolution of this asymmetry due to finite-depth effects is not well known, except that it is a slowly varying function of the steepness (Tayfun 2006; Tayfun & Alkhalidi 2020). To describe the change in vertical asymmetry due to bandwidth and relative water depth, we assess data from North Sea observations. Data were collected on Total Oil Marine's oil platform North Alwyn NAA located at $60°48.5'$ N and $1°44.2'$ E, approximately 135 km east of the Shetland Islands (Scotland) and 156 km west of the Norwegian coast (Stansell 2004, 2005). The platform sits on a depth of 129 m and on a mild slope of $\nabla h \sim -1/300$ in the SE-NW direction (according to bathymetry charts from EMODnet – European Marine Observation and Data Network, see figure 3). While the mean wave direction during the winter storms observed between 1995 and 1999
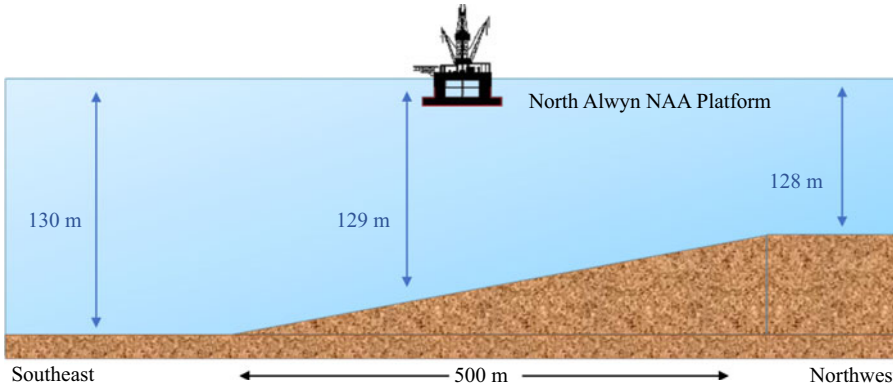
Figure 3. Approximate bathymetric features around the oil platform in the North Sea. The sketch is not to scale.

(Linfoot, Stansell & Wolfram 2000) is in the SE-NW direction, we focused on the shoaling case, i.e. waves coming from the southeast towards the northwest. The mild slope is almost linear ($\nabla^2 h \approx 0$) within a distance of 250 m northwest and southeast of the platform, corresponding to three mean wavelengths (see table 3 of Mendes *et al.* (2021) for the measurements). The raw data were stored as 2381 20 min records of surface elevation measurements recorded with a sampling rate of 5 Hz.

To perform the comparison with ocean data, we follow Marthinsen (1992) and consider the skewness of the surface elevation to depend solely on relative water depth and wave steepness $\mu_3 = \mu_3(\varepsilon, k_p h)$, and consequently identify $\mathfrak{S}(\mu_3) = \mathfrak{S}(\varepsilon, k_p h)$ for any α due to (2.6). We approximate the skewness as (see (19) of Tayfun (2006), where μ denotes steepness and λ_3 the skewness)

$$\mu_3(k_p h > \pi) \approx 3k_1\sigma(1 - \nu\sqrt{2} + \nu^2) \equiv 3k_1\sigma \cdot \mathfrak{B}(\nu) \approx \frac{\pi}{\sqrt{2}}\varepsilon\mathfrak{B}(\nu), \qquad (4.1)$$

where $H_s = \pi\varepsilon/\sqrt{2}k_p$ and k_p is the peak wavenumber obtained from the spectral mean wavenumber k_1 through $k_p \approx (3/4)k_1$ (Mendes *et al.* 2022) and ν is the spectral bandwidth (Longuet-Higgins 1975). In deep water ($k_p h \geq 5$), figure 4(*a*) shows that the skewness is almost independent of the bandwidth, as expected from (4.1). On the other hand, as the depth decreases to intermediate waters the ratio μ_3/ε significantly increases and tends to strongly depend on bandwidth. To account for this finite-depth effect, we rewrite (4.1) according to (11) of Tayfun & Alkhalidi (2020)

$$\mu_3 \approx \frac{\pi\varepsilon}{\sqrt{2}}\mathfrak{B}(\nu)\left(\tilde{\chi}_0 + \frac{\sqrt{\tilde{\chi}_1}}{2}\right), \qquad (4.2)$$

with notation $\tilde{\chi}_i$ from Mendes *et al.* (2022)

$$\tilde{\chi}_0 = \frac{\left[4\left(1 + \dfrac{2k_p h}{\sinh(2k_p h)}\right) - 2\right]}{\left(1 + \dfrac{2k_p h}{\sinh(2k_p h)}\right)^2 \tanh k_p h - 4k_p h}; \quad \frac{\sqrt{\tilde{\chi}_1}}{2} = \frac{3 - \tanh^2(k_p h)}{2\tanh^3(k_p h)}. \qquad (4.3a,b)$$

Although Tayfun and Alkhalidi's model provides a good fit of μ_3/ε for $k_p h > 3$, the sum $\tilde{\chi}_0 + \sqrt{\tilde{\chi}_1}/2$ stays close to unity for $k_p h \geq 2$. Hence, the larger values of the ratio μ_3/ε
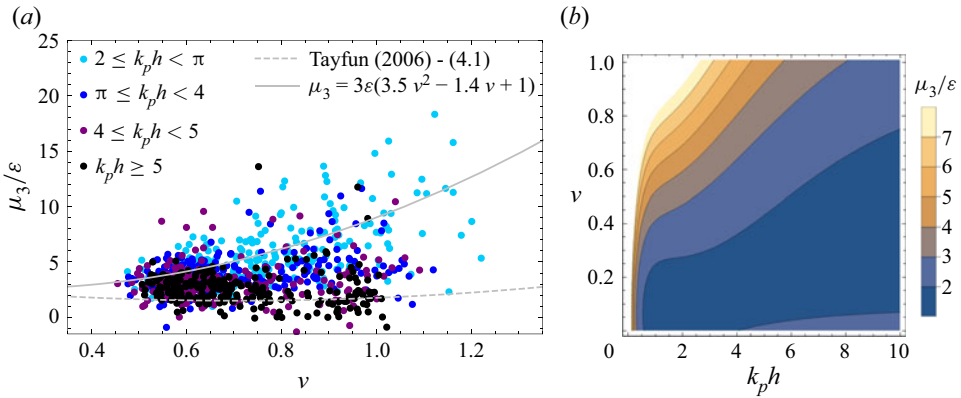
Figure 4. (*a*) Ratio of skewness and steepness varying with bandwidth in strongly non-Gaussian ($\mu_4 \approx 0.4$) North Sea data (Stansell 2004), with polynomial fit $\mathfrak{B}(\nu) \approx 1 - \nu\sqrt{2} + 3.5\nu^2$ at $2 \leq k_p h \leq \pi$. (*b*) Contour plot of the same ratio as computed from (4.2) for the fitted function $\mathfrak{B}(\nu, k_p h)$ in (*a*).

for shallower water ($2 \leq k_p h \leq \pi$) must stem from a dependence of $\mathfrak{B}(\nu)$ on depth. We therefore seek a generalization of (4.2) whereby we fit a function $\mathfrak{B}(\nu, k_p h) = 1 - \nu\sqrt{2} + f_{k_p h} \cdot \nu^2$ capable of providing a smooth transition from $f_{k_p h \sim 3} \approx 3.5$ in shallower depths (see figure 4*a*) to the deep water value $f_{k_p h = \infty} \sim 1$ (see (4.1)). Hence, implementing this fit into (2.6) and (2.7) the vertical asymmetry accounting for depth-induced effects is of the type

$$\mathfrak{S}(\alpha = 2) \approx \frac{(2 + 6\varepsilon_*)(7 + 3\varepsilon_*)}{6(2 + 3\varepsilon_*)}, \tag{4.4}$$

where ε_* is the effective steepness

$$\varepsilon_* \approx \frac{\pi\varepsilon}{3\sqrt{2}}[1 - \nu\sqrt{2} + f_{k_p h} \cdot \nu^2]\left(\tilde{\chi}_0 + \frac{\sqrt{\tilde{\chi}_1}}{2}\right). \tag{4.5}$$

Figure 4(*b*) provides a contour plot for the ratio μ_3/ε taking into account the fitted model of $f_{k_p h}$. Here, $f_{k_p h}$ is a function of depth that can be obtained through the constraint $\mathfrak{S} \leq 2$ of (2.5) applied to (4.4)

$$\lim_{k_p h \to 0} \mathfrak{S}(\alpha = 2) \approx \lim_{k_p h \to 0} \frac{(2 + 6\varepsilon_*)(7 + 3\varepsilon_*)}{6(2 + 3\varepsilon_*)} \leq 2, \tag{4.6}$$

thus leading to

$$9\varepsilon_*^2 + 6\varepsilon_* - 5 \leq 0 \quad \therefore \quad \varepsilon_* \leq \frac{\sqrt{6} - 1}{3}. \tag{4.7}$$

The function $\mathfrak{B}(\nu, k_p h)$ makes the exceedance probability of rogue waves weakly dependent on the bandwidth ν (Longuet-Higgins 1975). Very broad-banded seas ($\nu \geq 1$) are very rare. For example, they account for only 3 % of observed stormy states in the North Sea (Mendes *et al.* 2021). These extreme sea conditions are typically short lived and found for instance in hurricanes. Albeit bandwidths much larger than $\nu = 1$ can increase the vertical asymmetry by approximately 5 %–10 %, their lifespan impacts the weighted average of the exceedance probability of rogue waves over a daily forecast by only $\sim$10 %
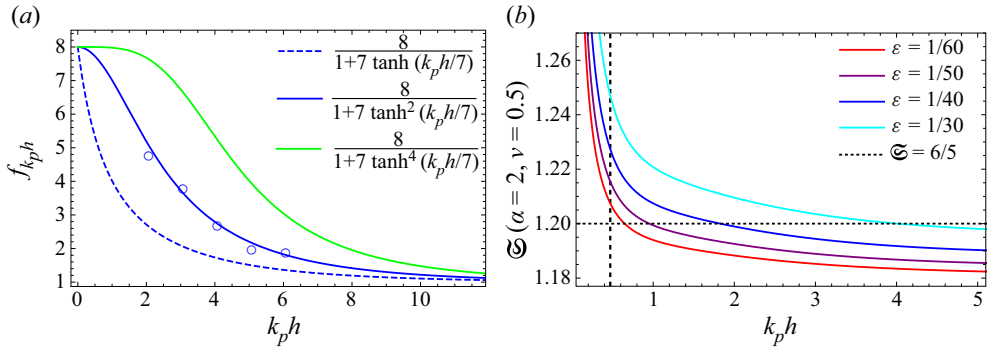
966 A42-8

Figure 5. (*a*) Finite-depth functions $f_{k_p h}$ vs data (circles) from figure 4(*a*). (*b*) Vertical asymmetry of broad-banded rogue waves ($\nu = 0.5$) as a function of water depth for different steepness, with the dotted line depicting the empirical mean value $\mathfrak{S} = 1.2$ from Mendes *et al.* (2021, 2022). Dashed vertical line marks the limit of validity of second-order theory.

because $\nu \sim 0.5$ over 97 % of all 30 min records. Accordingly, we may set $\nu = 1$ as the realistic and effective maximum bandwidth to be considered for estimating the rogue wave exceedance probability. Hence, in the second-order limit we obtain

$$\lim_{k_p h \to 1/2} \frac{\pi \varepsilon}{3\sqrt{2}} f_{k_p h} \left(\tilde{\chi}_0 + \frac{\sqrt{\tilde{\chi}_1}}{2} \right) < \frac{\sqrt{6} - 1}{3}. \qquad (4.8)$$

Consequently, broad-banded waves will not exceed the following depth correction:

$$f_{k_p h}(\nu = 1) \lesssim \frac{18\sqrt{2}}{\pi} \approx 8. \qquad (4.9)$$

Broad-banded waves have an effective steepness of the order of $\varepsilon f_{k_p h} \nu^2$. Since finite-depth effects involve the ratio $\varepsilon / k_p h$ which it is directly related to H_s / h and $f_{k_p h}$ grows quickly from deep to intermediate waters (see figure 4a), we expect $f_{k_p h}$ to be inversely proportional to the relative depth $k_p h$. In order to fulfil (4.6)–(4.9), a sigmoid function provides a good fit with continuous derivative for the North Sea data (see figure 5a)

$$f_{k_p h} \approx \frac{8}{1 + 7 \tanh^2 (k_p h / 7)}, \quad \nu \leq 1. \qquad (4.10)$$

Plugging (4.10) into (4.4) introduces an approximation for the vertical asymmetry covering the entire range of second-order theory for narrow and broad-banded irregular waves. In fact, figure 5(*b*) shows that the vertical asymmetry is almost constant for typical values of mean steepness ($\varepsilon \ll 1/10$) in intermediate and deep waters ($k_p h \geq \pi/10$). Conversely, sharp increases in the mean steepness will induce a few per cent increase in the vertical asymmetry in the same regimes ($k_p h \geq \pi/10$). The contour plot in figure 6(*b*) provides a full description of the variations in asymmetry with depth and steepness. Furthermore, figure 6(*a*) shows that, in shallow depths, the vertical asymmetry strongly depends on $k_p h$ while in deep water it tends to saturate. Figure 6(*c*) also illustrates the role of bandwidth in increasing the asymmetry, albeit sharp changes are restricted to sufficiently broad spectra ($\nu > 0.8$). Thus, the analysis of field data from the North Sea shows that, as long as the steepness in intermediate water ($k_p h > \pi/10$) is small ($\varepsilon < 1/10$) or the spectrum narrow ($\nu < 1/2$), the vertical asymmetry stays close to $\mathfrak{S} = 1.2$. We find this approximation for
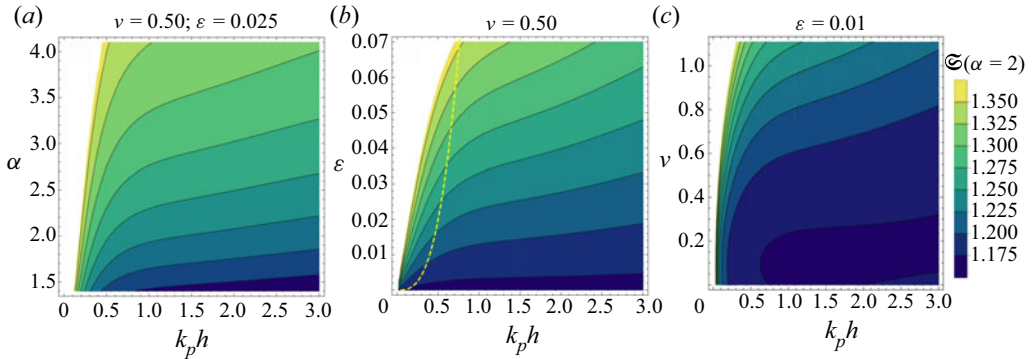
Figure 6. Vertical asymmetry of large and rogue waves as a function of water depth for different mean steepness, bandwidth and normalized height. The dashed line in (*b*) represents the Ursell limit for second-order theory.

the vertical asymmetry to be still applicable to the experiments in Trulsen *et al.* (2020) with steeper slope, as shown in Appendix B.

Moreover, the special case of narrow-banded ($\nu = 0$) linear waves ($\varepsilon \ll 1/10$) in deep water leads to $\varepsilon_* \to 0$, thus reaching the lower bound of the asymmetry $\mathfrak{S} = 7/6$ for rogue waves. This suggests that, in intermediate waters, narrowing the bandwidth from $\nu = 0.3$ to $\nu = 0$ will have little impact on the amplification of rogue wave statistics due to the negligible change in vertical asymmetry, whereas in shallow water increasing the bandwidth above $\nu = 0.5$ will significantly boost rogue wave occurrence. From the point of view of the theory in Mendes *et al.* (2022), the asymmetry approximation of (4.4), (4.10) explains why narrow-banded models (Li *et al.* 2021*a*) are successful in predicting rogue wave statistics travelling past a step in a broad-banded irregular wave background in intermediate water. Provided there is no wave breaking ($H_s/h \ll 1$), the bandwidth effect will play a role in amplifying statistics in shallower depths because of the contributuin of the term $f_{k_p h}\nu^2$, as experimentally demonstrated in Doeleman (2021).

5. Upper bound for kurtosis atop a shoal

The excess kurtosis has been used in the past two decades as a proxy for how rough nonlinear seas increase the occurrence and intensity of rogue waves. Therefore, in this section we extend our results of § 3 to estimate the maximum kurtosis atop any shoal in the ocean (Janssen & Bidlot 2009; Janssen 2017). The assessment of maximum expected waves over a specific return time at a fixed location is crucial for naval design. Typically, ocean structures and vessels must be designed to sustain expected maximum extreme waves over their lifespan (Borgman 1973; Muir & El-Shaarawi 1986). In order to do so, we shall evaluate maxima for the parameters $\mathfrak{S}$ and Γ. Equations (4.4) and (4.10) provide the upper bound for the vertical asymmetry of rogue waves in the limit of wave breaking: $\mathfrak{S}_\infty(k_p h = \infty) \approx 1.387$ in deep water and $\mathfrak{S}_\infty(k_p h = 0) \approx 1.668$ in shallow water. Since the Γ correction is also limited by wave breaking, one finds the bound $\Gamma_\infty - 1 \lesssim 1/12$ due to (3.17) of Mendes *et al.* (2022). Hence, we may approximate

$$1 - \frac{1}{\mathfrak{S}_\infty^2 \Gamma_\infty} \lesssim 8(\Gamma_\infty - 1). \tag{5.1}$$

Approaching the value Γ_∞ atop the shoal (region III of figure 1), the contribution of the skewness to the amplification of wave statistics near the breaking regime increases such
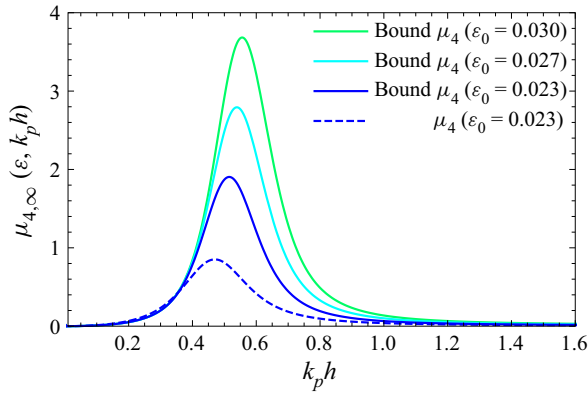
966 A42-10

Figure 7. Upper bound on kurtosis from (5.3) for $\nu = 0.5$ and different pre-shoal mean (significant) steepness $\varepsilon_0 = H_{s,0}/\lambda_0$ subject to linear shoaling. The dashed curve represents the kurtosis in figure 2(*a*), representative of run 1 of Trulsen *et al.* (2020) and with the bathymetry of figure 1.

that the relationship between kurtosis and skewness leading to (3.2) is modified and now empirically reduces to $\mu_4 \approx \mu_3^2$ (Ma *et al.* 2015). Plugging this relationship into (3.1) and comparing it with (2.4) and (5.1), we obtain

$$\exp(16\alpha^2(\Gamma_\infty - 1)) \geq 1 + \alpha^2(\alpha^2 - 1)\mu_4. \tag{5.2}$$

At $\alpha = 2$, the evaluation of the excess kurtosis lies at the region of stability of the Gram–Charlier series and we are able to compute the upper bound for the excess kurtosis in the case of pre-shoal Gaussian statistics (see figure 7)

$$\mu_{4,\infty} \approx \tfrac{1}{12}[\exp(64(\Gamma_\infty - 1)) - 1], \tag{5.3}$$

where Γ_∞ varies with water depth. According to (5.3), typical seas with steep and highly asymmetrical broad-banded waves lead to an upper bound for the excess kurtosis of the order of $\mu_{4,\infty} \sim 4$ in intermediate water, see figure 7. We already described that the maximum value of Γ is located around $k_p h \approx 0.5$ in Mendes *et al.* (2022) and (3.3) has been validated in figure 2. Therefore, the peak in excess kurtosis will also be located in this region. Experiments conducted in Zhang *et al.* (2023) found the peak in excess kurtosis in the same region $k_p h \approx 0.5$.

6. Conclusions

In this work we have extended the framework in Mendes *et al.* (2022) to an effective theory for the evolution of excess kurtosis of the surface elevation over a shoal of finite and constant steep slope. We find quantitative agreement with experiments in Trulsen *et al.* (2020) regarding the magnitude of the kurtosis increase during and atop the shoal. While the groundwork of Marthinsen (1992) computes the excess kurtosis directly from the solution $\zeta(x, t)$, our model unravels the kurtosis dependence on the inhomogeneities of the energy density over a shoal. Our formulation outperforms the conventional method of Marthinsen (1992) for the computation of kurtosis of the bound wave contribution. In addition, our effective theory is capable of describing changes of the kurtosis magnitude over arbitrary slopes provided reflection can be neglected. A computation of the kurtosis from the probability density of $\zeta(x, t)$ through the non-homogeneous framework will be pursued in a future work with an analytical non-uniform distribution of random phases.

Furthermore, we have obtained an approximation for the vertical asymmetry in finite depth as a function of both steepness and bandwidth. This approximation extends the seminal work of Tayfun (2006) for the skewness of the surface elevation to broad-banded intermediate water waves while recovering its original formulation for narrow-banded deep water waves. Building on this new approximation, we have demonstrated that the vertical asymmetry varies slowly over a shoal in both deep and intermediate waters. Moreover, based on this rise in vertical asymmetry we were able to compute an upper bound for the excess kurtosis driven by shoaling.

Declaration of interests. The authors report no conflict of interest.

Author ORCIDs.
S. Mendes https://orcid.org/0000-0003-2395-781X;
J. Kasparian https://orcid.org/0000-0003-2398-3882.

Appendix A. Computation of irregular bound wave kurtosis

The contribution of bound waves to the excess kurtosis of the surface elevation is given by Mori & Kobayashi (1998) in the regular wave approximation

$$\mu_4(ka, kh) = 3 \left\{ \frac{1 + (ka)^2(6D_1^2 + 6D_2^2 + 8D_1D_2)]}{[1 + (ka)^2(D_1^2 + D_2^2)]^2} - 1 \right\}, \tag{A1}$$

where D_1 and D_2 are relative water depth coefficients from the surface elevation

$$D_1 = \frac{1}{\tanh kh}; \quad D_2 = D_1 \left(1 + \frac{3}{2 \sinh^2 kh} \right). \tag{A2a,b}$$

To leading order in steepness, we may approximate the excess kurtosis as

$$\begin{aligned} \mu_4 &\approx 3\{[1 + (ka)^2(6D_1^2 + 6D_2^2 + 8D_1D_2)][1 - 2(ka)^2(D_1^2 + D_2^2)] - 1\}, \\ &\approx 3\{[1 + (ka)^2(4D_1^2 + 4D_2^2 + 8D_1D_2)] - 1\}, \\ &\approx 3(ka)^2(4D_1^2 + 4D_2^2 + 8D_1D_2) \approx 12(ka)^2(D_1 + D_2)^2. \end{aligned} \tag{A3}$$

However, we shall extend (A1) for irregular waves, computing the equivalent irregular mean wave steepness and relative depth. We may use $ka \to k_p H_s/2\sqrt{2}$ as pointed out in Trulsen *et al.* (2020) for irregular waves, consequently we find $ka \to (\pi/4)\varepsilon$ as in Mendes *et al.* (2022). Hence, we may write the excess kurtosis as a function of ε up to second order in steepness

$$\mu_4 \approx \frac{3\pi^2}{4} \cdot \varepsilon^2(D_1 + D_2)^2. \tag{A4}$$

Moreover, the depth kh has to be converted to its peak wavenumber equivalent $k_p h$. Hence, since observations in the ocean feature $1.1 \le \lambda_p/\lambda_{1/3} \le 1.2$ (Figueras 2010), we may use the transformation from regular wave to irregular wave $kh \to 1.2k_p h$ to compute (D_1, D_2) correctly. As a remark, the above expression differs little from formulations such as of Marthinsen (1992) and others as reviewed in Tayfun & Alkhalidi (2020).
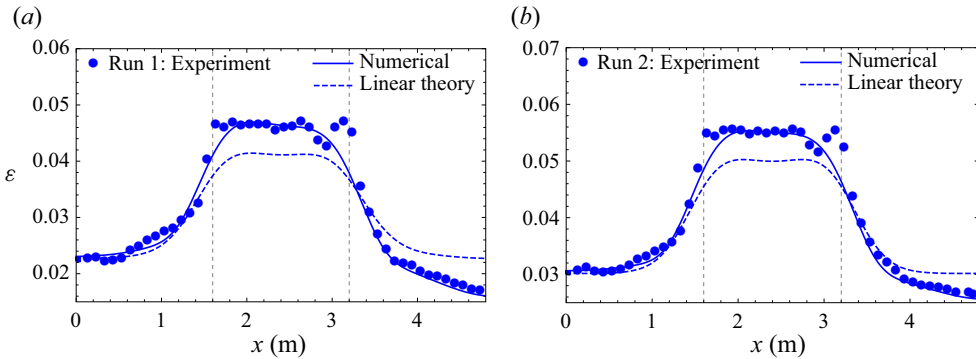
Figure 8. Theoretical evolution of steepness measured against observations (dots) in Raustøl (2014) and its numerical fit thereof for (*a*) run 1 and (*b*) run 2 of the experiments in Trulsen *et al.* (2020).

Appendix B. Slope effect on vertical asymmetry

In this section we assess how the vertical asymmetry of irregular rogue waves is affected by an arbitrary slope. Let us denote the final steepness atop the shoal as ε_f and the initial one as ε_0. If linear waves travel over a shoal, then we may define the amplification ratio of the steepness (also known as shoaling coefficient)

$$K_{\varepsilon,\mathrm{L}} := \frac{\varepsilon_f}{\varepsilon_0} \approx \frac{1}{\tanh\left(1.2 k_p h\right)} \left[\frac{2 \cosh^2\left(1.2 k_p h\right)}{2.4 k_p h + \sinh\left(2.4 k_p h\right)} \right]^{1/2}, \tag{B1}$$

where we have converted the regular wave formula (Holthuijsen 2007) to irregular waves. Indeed, except for a few per cent, the shoaling coefficient of the (irregular) significant wave height is a good approximation for the regular wave counterpart (Goda 1975, 2010). If nonlinear wave shoaling is dominant, then $K_{\varepsilon,NL}$ depends on the slope of the shoal ∇h, and we denote the ratio $K_{\varepsilon,NL}/K_{\varepsilon,L} = \mathcal{F}_{\nabla h}$ (Eagleson 1956; Walker & Headlam 1983; Srineash & Murali 2018). Performing a Taylor expansion in (4.4) up to first order in ε_*, the vertical asymmetry of small wave amplitudes can be written as

$$\mathfrak{S}(\alpha = 2) \approx \tfrac{7}{6}\left(1 + 2\varepsilon_*\right). \tag{B2}$$

The typical sea representative of Trulsen *et al.* (2020) experiments is broad-banded ($\nu \sim 0.5$) and in intermediate water ($k_p h \sim 1$). Recalling (4.5) and (4.10), this leads to $\mathfrak{B}(\nu) \sim 2$ and $\tilde{\chi}_0 + \sqrt{\tilde{\chi}_1}/2 \sim 1$. Therefore we may approximate $\varepsilon_* \approx (\pi\sqrt{2}/3)\varepsilon$. Consequently, the ratio between the vertical asymmetry of identical sea states of waves travelling over a shoal of different slopes is approximately described by the formula

$$\frac{\mathfrak{S}(\alpha = 2, |\nabla h|)}{\mathfrak{S}(\alpha = 2, |\nabla h| = 0)} \approx \frac{\left(1 + \dfrac{2\sqrt{2}\pi}{3}\varepsilon \cdot \mathcal{F}_{\nabla h}\right)}{\left(1 + \dfrac{2\sqrt{2}\pi}{3}\varepsilon\right)} \approx 1 + \frac{2\sqrt{2}\pi}{3}\varepsilon\left(\mathcal{F}_{\nabla h} - 1\right). \tag{B3}$$

Even for relatively steep shoals ($|\nabla h| \approx 1/4$) as in the case of Trulsen *et al.* (2020) the correction accounting for slope is small, with $\mathcal{F}_{\nabla h} \approx 1.15$ in this case (see figure 8*a,b*). In fact, Srineash & Murali (2018) demonstrated experimentally that $\mathcal{F}_{\nabla h} - 1$ stays in the range of 0.1–0.2 for steep slopes. Since the steepness in the experiments of

Trulsen *et al.* (2020) atop the shoal does not exceed $\varepsilon = 0.06$, the slope correction to the vertical asymmetry derived with the help of field data from the North Sea stays below $(\pi\sqrt{2}/9) \times 100\,\% \times 0.06 = 3\,\%$. Thus, (4.4) is applicable to the analysis in § 3, and the approximation $\mathfrak{S} \approx 1.2$ is applicable in the conditions of the experiments in Trulsen *et al.* (2020).

REFERENCES

AKHMEDIEV, N., ANKIEWICZ, A. & TAKI, M. 2009 Waves that appear from nowhere and disappear without a trace. *Phys. Lett.* A **373** (6), 675–678.

BATTJES, J.A. 1974 Surf similarity. *Coast. Engng Proc.* **1** (14), 26.

BITNER, E.M. 1980 Non-linear effects of the statistical model of shallow-water wind waves. *Appl. Ocean Res.* **2** (2), 63–73.

BOLLES, C.T., SPEER, K. & MOORE, M.N.J. 2019 Anomalous wave statistics induced by abrupt depth change. *Phys. Rev. Fluids* **4** (1), 011801.

BORGMAN, L.E. 1973 Probabilities for highest wave in hurricane. *J. Waterways Harbors Coast. Engng Div. ASCE* **99** (2), 185–207.

CASAS-PRAT, M. & HOLTHUIJSEN, L.H. 2010 Short-term statistics of waves observed in deep water. *J. Geophys. Res.* **115** (9), C09024.

CLAUSS, G.F. 2002 Dramas of the sea: episodic waves and their impact on offshore structures. *Appl. Ocean Res.* **24**, 147–161.

DOELEMAN, M.W. 2021 Rogue waves in the Dutch North Sea. Master's thesis, TU Delft.

DUCROZET, G. & GOUIN, M. 2017 Influence of varying bathymetry in rogue wave occurrence within unidirectional and directional sea-states. *J. Ocean Engng Mar. Energy* **3** (4), 309–324.

EAGLESON, P.S. 1956 Properties of shoaling waves by theory and experiment. *Eos* **37** (5), 565–572.

FIGUERAS, A.A. 2010 Estimation of available wave power in the near shore area around Hanstholm Harbor. Project of Special Thesis, Universidad Politecnica de Catalunya.

FORRISTALL, G.Z. 1978 On the distributions of wave heights in a storm. *J. Geophys. Res.* **83**, 2353–2358.

GLUKHOVSKIY, B.K. 1966 *Investigation of Sea Wind Waves* (in Russian). Gidrometeoizdat.

GODA, Y. 1975 Irregular wave deformation in the surf zone. *Coast. Engng Japan* **18** (1), 13–26.

GODA, Y. 1983 A unified nonlinearity parameter of water waves. *Rep. Port Harbour Res. Inst.* **22** (3), 3–30.

GODA, Y. 2010 *Random Seas for Design of Maritime Structures*. World Scientific.

HAVER, S. 2004 A possible freak wave event measured at the Draupner Jacket January 1 1995. In *Proc. Rogue Waves*, IFREMER.

HOLTHUIJSEN, L.H. 2007 *Waves in Oceanic and Coastal Waters*. Cambridge University Press.

JANSSEN, P.A.E.M. 2017 *Shallow-Water Version of the Freak Wave Warning System*. European Centre for Medium Range Weather Forecasts.

JANSSEN, P.A.E.M. & BIDLOT, J.-R. 2009 *On the Extension of the Freak Wave Warning System and its Verification*. European Centre for Medium-Range Weather Forecasts Reading.

KARMPADAKIS, I., SWAN, C. & CHRISTOU, M. 2020 Assessment of wave height distributions using an extensive field database. *Coast. Engng* **157**, 103630.

KARMPADAKIS, I., SWAN, C. & CHRISTOU, M. 2022 A new wave height distribution for intermediate and shallow water depths. *Coast. Engng* **175**, 104130.

KIMMOUN, O., HSU, H.-C., HOFFMANN, N. & CHABCHOUB, A. 2021 Experiments on uni-directional and nonlinear wave group shoaling. *Ocean Dyn.* **71**, 1105–1112.

LI, Y., DRAYCOTT, S., ZHENG, Y., LIN, Z., ADCOCK, T.A.A. & VAN DEN BREMER, T.S. 2021*a* Why rogue waves occur atop abrupt depth transitions. *J. Fluid Mech.* **919**, R5.

LI, Y., ZHENG, Y., LIN, Z., ADCOCK, T.A. & VAN DEN BREMER, T. 2021*b* Surface wavepackets subject to an abrupt depth change. Part 1. Second-order theory. *J. Fluid Mech.* **915**, A71.

LINFOOT, B., STANSELL, P. & WOLFRAM, J. 2000 On the characteristics of storm waves. *Proc. Intl Offshore Polar Engng Conf.* **3**, 74–83.

LONGUET-HIGGINS, M.S. 1952 On the statistical distribution of the heights of sea waves. *J. Mar. Res.* **11**, 245–265.

LONGUET-HIGGINS, M.S. 1963 The effect of non-linearities on statistical distributions in the theory of sea waves. *J. Fluid Mech.* **17**, 459–480.

LONGUET-HIGGINS, M.S. 1975 On the joint distribution of the periods and amplitudes of sea waves. *J. Geophys. Res.* **80** (18), 2688–2694.

MA, Y.-X., MA, X.-Z. & DONG, G.-H. 2015 Variations of statistics for random waves propagating over a bar. *J. Mar. Sci. Technol.* **23** (6), 864–869.

MARTHINSEN, T. 1992 On the statistics of irregular second-order waves. *Tech. Rep.* RMS-11.

MENDES, S. 2020 On the statistics of oceanic rogue waves in finite depth: exceeding probabilities, physical constraints and extreme value theory. PhD Thesis, University of North Carolina at Chapel Hill, NC.

MENDES, S. & KASPARIAN, J. 2022 Saturation of rogue wave amplification over steep shoals. *Phys. Rev.* E **106**, 065101.

MENDES, S., SCOTTI, A., BRUNETTI, M. & KASPARIAN, J. 2022 Non-homogeneous model of rogue wave probability evolution over a shoal. *J. Fluid Mech.* **939**, A25.

MENDES, S., SCOTTI, A. & STANSELL, P. 2021 On the physical constraints for the exceeding probability of deep water rogue waves. *Appl. Ocean Res.* **108**, 102402.

MOORE, N.J., BOLLES, C.T., MAJDA, A.J. & QI, D. 2020 Anomalous waves triggered by abrupt depth changes: laboratory experiments and truncated KDV statistical mechanics. *J. Nonlinear Sci.* **30** (6), 3235–3263.

MORI, N. & JANSSEN, P.A.E.M. 2006 On kurtosis and occurrence probability of freak waves. *J. Phys. Oceanogr.* **36** (7), 1471–1483.

MORI, N. & KOBAYASHI, N. 1998 Nonlinear distribution of nearshore free surface and velocity. In *Coastal Engineering 1998*, pp. 189–202.

MORI, N. & YASUDA, T. 2002 A weakly non-Gaussian model of wave height distribution random wave train. *Ocean Engng* **29** (10), 1219–1231.

MUIR, L.R & EL-SHAARAWI, A.H. 1986 On the calculation of extreme wave heights: a review. *Ocean Engng* **13** (1), 93–118.

RAUSTØL, A. 2014 Freake bølger over variabelt dyp. Master's thesis, University of Oslo.

RICE, S.O. 1945 Mathematical analysis of random noise. *Bell Syst. Tech. J.* **24** (1), 46–156.

SRINEASH, V.K. & MURALI, K. 2018 Wave shoaling over a submerged ramp: an experimental and numerical study. *ASCE J. Waterway Port Coast. Ocean Engng* **144** (2), 04017048.

STANSELL, P. 2004 Distribution of freak wave heights measured in the north sea. *Appl. Ocean Res.* **26**, 35–48.

STANSELL, P. 2005 Distributions of extreme wave, crest and trough heights measured in the north sea. *Ocean Engng* **32**, 1015–1036.

TAYFUN, M.A. 1980 Narrow-band nonlinear sea waves. *J. Geophys. Res.* **85**, 1548–1552.

TAYFUN, M.A. 1990 Distribution of large wave heights. *ASCE J. Waterway Port Coast. Ocean Engng* **116** (6), 686–707.

TAYFUN, M.A. 2006 Statistics of nonlinear wave crests and groups. *Ocean Engng* **33** (11), 1589–1622.

TAYFUN, M.A. & ALKHALIDI, M.A. 2020 Distribution of sea-surface elevations in intermediate and shallow water depths. *Coast. Engng* **157**, 103651.

TEUTSCH, I., WEISSE, R., MOELLER, J. & KRUEGER, O. 2020 A statistical analysis of rogue waves in the southern north sea. *Nat. Hazards Earth Syst. Sci.* **20** (10), 2665–2680.

TOFFOLI, A., WASEDA, T., HOUTANI, H., CAVALERI, L., GREAVES, D. & ONORATO, M. 2015 Rogue waves in opposing currents: an experimental study on deterministic and stochastic wave trains. *J. Fluid Mech.* **769**, 277–297.

TRULSEN, K., RAUSTØL, A., JORDE, S. & RYE, L.B. 2020 Extreme wave statistics of long-crested irregular waves over a shoal. *J. Fluid Mech.* **882**, R2.

TRULSEN, K., ZENG, H. & GRAMSTAD, O. 2012 Laboratory evidence of freak waves provoked by non-uniform bathymetry. *Phys. Fluids* **24** (9), 097101.

WALKER, J. & HEADLAM, J. 1983 Engineering approach to nonlinear wave shoaling. *Proc. Coast. Engng Conf.* **1**, 523–542.

ZHANG, J., BENOIT, M., KIMMOUN, O., CHABCHOUB, A. & HSU, H.-C. 2019 Statistics of extreme waves in coastal waters: large scale experiments and advanced numerical simulations. *Fluids* **4** (2), 99.

ZHANG, J., MA, Y., TAN, T., DONG, G. & BENOIT, M. 2023 Enhanced extreme wave statistics of irregular waves due to accelerating following current over a submerged bar. *J. Fluid Mech.* **954**, A50.